Open access • Journal Article • DOI:10.1007/S003390050025

Formation of cluster-assembled carbon nano-foam by high-repetition-rate laser ablation — Source link

Andrei Rode, Eugene G Gamaly, Barry Luther-Davies

Institutions: Australian National University, Universidad Autónoma Metropolitana

Published on: 01 Feb 2000 - Applied Physics A (Springer)

Topics: Amorphous carbon, Carbon film, Carbon, Carbon nanofoam and Amorphous solid

Appl. Phys. A 70, 135–144 (2000) / Digital Object Identifier (DOI) 10.1007/s003390000252

Applied Physics A
Materials
Science & Processing

Formation of cluster-assembled carbon nano-foam by high-repetition-rate laser ablation

A.V. Rode[1], **E.G. Gamaly**[2,*], **B. Luther-Davies**[1]

[1] Laser Physics Centre, Research School of Physical Science and Engineering, Australian National University, Canberra, ACT 0200, Australia
(Fax: +61-2/6249-0029, E-mail: avr111@rsphy1.anu.edu.au; bld111@rsphy1.anu.edu.au)
[2] Departamento de Fisica, Universidad Autonoma Metropolitana–Iztapalapa, Apartado Postal 55-534, 09340, Mexico D.F., Mexico
(Fax: +52-5/72-4611, E-mail: egg@xanum.uam.mx)

Received: 6 May 1999/Accepted: 8 September 1999/Published online: 21 January 2000 –

Abstract. High-repetition-rate laser ablation and deposition of carbon vapours results in the formation of quite different carbonaceous structures depending on the pressure of the ambient Ar gas in the chamber. Diamond-like carbon films form at a pressure below ≈ 0.1 Torr whereas a diamond-like carbon nano-foam is created above 0.1 Torr. Although laser-deposited amorphous carbon films have been extensively investigated in the past, here we present what, to our knowledge, is the first report of the production of a granular low-density carbon nano-foam with rich fraction of sp^3 bonding. The bulk density of various foam samples was in the range $(2–10)\times10^{-3}$ g/cm^3, and the specific surface area was 300–400 m^2/g. The resistivity of the foam measured at low-voltage (±30 V) is $(1–3)\times10^9$ Ohm cm at room temperature and $(1–10)\times10^{13}$ Ohm cm at 80 K. The dc conductivity of this low-density carbon foam and its temperature dependence appears to be very close to that of RF-sputtered solid amorphous diamond-like carbon films.

The presented kinetic analysis of the carbon vapour in the Ar ambient demonstrates qualitative agreement between the predicted laser plume parameters and those measured in the experiments. Theoretical predictions of the parameters and the process of carbon vapour diffusion through the ambient gas, allow us to propose a self-consisted periodic model leading to the formation of the carbon clusters in the experimental chamber.

PACS: 81.15.F; 61.46; 73.61.Tm

The creation of particular molecular structures involves "atom-to-atom" attachment in appropriate physical conditions at an appropriate rate. In this context, laser ablation of graphite by conventional ns, 10–30 Hz, high-energy lasers has been quite successfully applied to the formation of the nanometric structures such as fullerenes C_{60} [1], and carbon nanotubes [2], which have many remarkable electrical, optical, and mechanical properties. Similar lasers have been used for around three decades to create thin solid films by laser ablation from solid targets.

Quite recently it has been suggested and demonstrated that very efficient evaporation of laser-irradiated targets and deposition of thin films can be obtained using rather different laser sources, namely short (as short as a few fs) low-energy (μJ) pulses delivered at high repetition rates (10 kHz–100 MHz) [3–5]. Using such lasers, the number of particles evaporated by a single laser pulse is reduced by many orders of magnitude compared with that produced by conventional high-energy laser pulses. This almost completely eliminates the ejection of large particulates from the target, which, in turn, eliminates particle contamination of the deposited film. In spite of the small number of atoms evaporated by a single laser pulse, high deposition rates can be achieved because of the compensating effect of the high-repetition-rate and through the use of optimal evaporation conditions. We show here that high repetition rate laser evaporation also increases the average temperature of the material arriving at the substrate by up to 20 times compared with conditions using conventional lasers, thus producing better conditions for the formation of nanostructures.

A significant advantage of the ablation using high-repetition-rate, low-energy pulses over the conventional systems follows from the additional degree of control over the state of the vapour produced in the experimental chamber. Controllable parameters in the experiments include the laser pulse duration and pulse energy as well as the time delay between the pulses. As the repetition rate increases quasi-steady conditions can exist. At sufficiently high repetition rates (> a few kHz), the spread in thermal velocities of the evaporated material is such that the atoms evaporated from one pulse overlap in space with those evaporated by previous pulses. In such quasi-continuous evaporation conditions, the chamber pressure stabilises at the point where evaporation balances either the pumping rate from the chamber, or particle loss to deposition on the chamber surfaces, or due to molecule-building interactions. By varying additional parameters such as the pressure of an inert gas in the chamber, a volume of energetic interacting particles with varying density and temperature can be created, providing a controllable environment for the growth of nanostructures.

Current address: Department of Applied Mathematics, Research School of Physical Science and Engineering, Australian National University, Canberra, ACT 0200, Australia
(Fax: +61-2/6249-0732, E-mail: gam110@rsphysse.anu.edu.au)

In what follows we concentrate on the defining the properties of the atomic vapours (plasma) ablated using high-repetition-rate lasers, and attempt to relate these to the properties of the material produced on a substrate.

The paper is organised as follows. Section 1 describes the experimental set-up and the characteristics of the carbon plume. We describe the experimental conditions required for the formation of a low-density carbon foam as well as its properties. In Sect. 2 we present a theoretical description of conditions in the laser plume under different regimes of laser–target interaction. The ionisation state of the plume, and the threshold intensity for the transition of the laser plume from neutral transparent vapour to opaque plasma are established. Furthermore, we estimate the temperature at the vapour–target surface boundary, the evaporation rate, and the vapour density as a function of laser intensity and target parameters during the target evaporation by a single pulse. Then, the average temperature of the substrate surface, the evaporation and deposition rates are calculated for the laser–target interaction for repetitive pulses and compared to that of experiment in Sect. 3. In Sect. 4 we discuss the results and make conclusions.

1 Experiments

1.1 Experimental set-up and laser plume parameters

A 42-W, 120-ns pulse-width Q-switched Nd:YAG laser ($\lambda = 1.064\,\mu$m) with variable repetition rate 2–25 kHz was used for ablation of glassy carbon in vacuum and in ambient Ar gas. The intensity of $\approx 10^9$ W/cm^2 averaged over the pulse duration was created in the focal spot $S_{\rm foc} = 2 \times 10^{-5}$ cm^2 on a target. In these experiments the repetition rate was fixed at 10 kHz, and the focal spot was scanned over a 2×2 cm area of the target surface. The measurements of absorption for the glassy carbon target gave the absorption coefficient of $A \approx 0.85$. The measured evaporation rate for a single 120-ns pulse constitutes $R_{\rm evap} = (1.4 \pm 0.2) \times 10^{26}$ atoms/cm^2 s. The detailed description of experimental installation and the laser plume diagnostics used was published in [5].

Time-integrated, space-resolved, target surface temperatures were measured for 120-ns, 10-kHz laser ablation. The target surface temperature was $2600\,\mathrm{K} \pm 50\,\mathrm{K}$ in the focal spot of diameter $\approx 50\,\mu$m. Optical images of the carbon plume in vacuum indicate a wide cone with its vertex in the focal spot and the cone angle of $\approx 120°$. The angular distribution of the ablated carbon vapour was measured from variations in the thickness of the deposited carbon film and the thickness measurements were performed by means of optical ellipsometry. The fit to the experimental data suggest the source distribution was $f(\theta) \approx \cos^{0.75}(\theta)$. Such angular distribution contrasts with a narrow-angle "pencil-shaped" plume from conventional high-pulse-energy low-repetition-rate laser ablation. The broad distribution for the case presented here follows from the fact that the focal spot is very small relative to the target–substrate distance.

The emission spectra of the target surface and the laser plume in vacuum (Fig. 1a) and in 100-Torr Ar ambient (Fig. 1b) were recorded in the 200–800 nm spectral range. The spectrum in vacuum (Fig. 1a) consists of two easily distinguished parts: one continuous radiation above 600 nm, and the other line radiation below 400 nm from the carbon vapour. The continuous spectrum fits well with the Plank's radiation law for a temperature range of 2500 K to 3500 K. This temperature range is above the carbon sublimation temperature ≈ 2500 K at the vacuum $\approx 10^{-6}$ Torr in the chamber [6]. The most intense spectral lines, located at 251, 258, 275, 284, 299, 388–392 nm were identified as CII emission (ionisation potential 11.26 eV), and those located at 216, 230, 270–272 nm were identified as CIII emission (ionisation potential 24.38 eV). The spectral lines' intensities varied during the evaporation. Nevertheless, the general behaviour was as follows. There is rather weak radiation from neutral carbon (CI) at 248 nm along with the equally intense lines from the singly ionised (CII) and doubly ionised (CIII) carbon ions. On the basis of these observations we can roughly estimate the temperature in the radiating carbon plasma as $1.5\,\mathrm{eV} \le kT_{\rm b} \le 6\,\mathrm{eV}$.

It should be noted that the carbon spectrum of the laser plume produced by high-repetition-rate laser in vacuum does not exhibit the bands of the well-known "Swan system" which correspond to vibrational modes of C_2 molecular radiation. The presence of the Swan bands is typical for a laser-produced plume with conventional low-repetition-rate high pulse power laser ablation [7–9]. The absence of C_2 molecules in the plasma plume constitutes the evidence of collisionless expansion of the carbon vapours. This characteristic, together with a wide-angle distribution of the evaporated carbon atoms, is a distinguished feature of a low-density, high-temperature plume produced in the high-repetition-rate laser ablation in vacuum with a relatively small number of atoms evaporated per single laser pulse.

By contrast, the laser plume emission spectra in Ar are dominated by the Swan bands of C_2 radicals (Fig. 1b) appearing on a top of the intense continuous radiation in the long-wavelength part of the spectra. The recorded Swan bands included $\Delta v = +1$ (470–475 nm); $\Delta v = 0$ (510–516 nm);

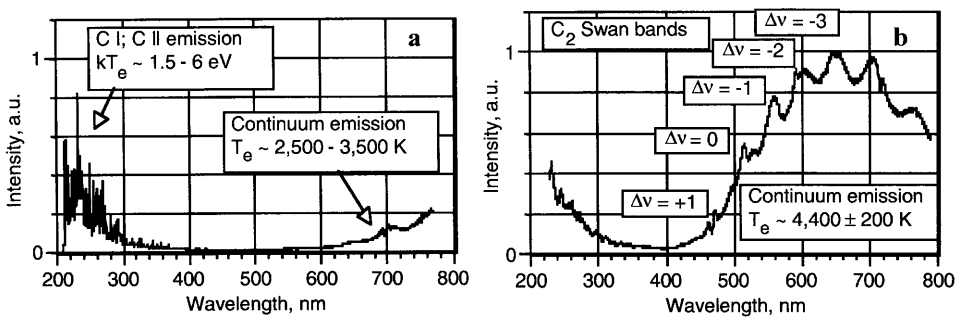

Fig. 1a,b. Optical emission spectra of the carbon plume produced with a high repetition rate laser in vacuum (**a**) and in Ar ambient at 100 Torr (**b**). In vacuum the spectrum is featureless between 400 nm and 600 nm indicating the absence of C_2 molecules in the plume (**a**). In Ar the spectrum is dominated by the Swan bands of C_2 molecules (**b**) on top of continuous radiation with a maximum at ≈ 650 nm

$\Delta v = -1$ (550–565 nm); $\Delta v = -2$ (595–615 nm) and $\Delta v = -3$ (650–665 nm); where Δv is the difference of the vibrational quantum numbers between the upper and the lower states of transition [10]. The peaks at ≈ 710 nm and at ≈ 780 nm could be attributed to high-pressure bands excited at relatively high pressures (10–100 Torr), which are parts of the Swan system with $\Delta v = -4$ and $\Delta v = -5$ correspondingly, and with the vibrational upper level 6 [10]. Together with the C_2 Swan bands, a weak radiation from atomic carbon CI (248, 477, 538, 600 nm), single-ionised CII (283, 515, 589, 685, 723 nm), and double-ionised CIII (230, 270–272, 465 nm) carbon ions was also detected. There was no detectable ArI emission, similar to the results on carbon evaporation in Ar with KrF laser at almost the same laser intensity [9]. The background continuous radiation fits well the Plank's radiation law for a temperature range 4400 ± 200 K. For 100 Torr, the carbon sublimation temperature is 4100 K [6].

The theoretical analysis of the ionisation processes in the laser plume, depending on the laser intensity, wavelength, and pulse duration is presented below in Sect. 2.1.

1.2 Carbon foam formation in Ar *ambient*

The diamond-like carbon (DLC) films were deposited in the vacuum of $\approx 10^{-6}$ Torr [5]. Transformation to a different form of carbon material occurs in an Ar-filled chamber at a pressure around 0.1 Torr. At this pressure the Ar number density in the chamber is $\approx 3 \times 10^{15}$ cm^{-3}, and the mean free path for collisions of the evaporated carbon atoms is in the order of 1 cm. Thus, carbon–carbon and carbon–argon collisions in the chamber start to play a dominant role in the formation of carbonaceous structures in Ar-filled chamber. The high-repetition-rate laser evaporation of a carbon target in a 1–100 Torr Ar atmosphere produces a higher evaporation rate of carbon atoms and ions than conventional laser ablation techniques. The resulting increased average temperature and density of the carbon/argon mixture in the experimental chamber increases the probability of the formation of higher energy carbon–carbon bonds. The increased collision frequency resulting from these deposition conditions encourages diffusion-limited aggregation of carbon atoms into fractal structures, and the formation of a low-density carbon foam.

The analysis of the scanning and transmission electron microscope images revealed that the foam represents a fractal-like structure which consists of carbon clusters with the average diameter of 6 nm randomly interconnected into a web-like foam (Fig. 2). The foam looks like a capricious mixture of "strings of pearls". At this stage it is difficult to resolve if these clusters are closed or open (cage-like) structures. Preliminary mass spectroscopy of the foam has shown a broad peak 35 000–60 000 a.m.u. with the maximum at $\approx 50\,000$ a.m.u., i.e. the dominant cluster contains $\approx 4 \times 10^3$ carbon atoms. Attributing this weight to a 6-nm cluster one obtains the average cluster density of 0.73 g/cm^3. Multipoint Brunauer–Emmett–Teller (BET) surface area measurements revealed that the surface area of the foam is in the range 300–400 m^2/g. The bulk density of the *a*-C foam samples, determined from He^+ ion backscattering measurements of the areal carbon density and scanning electron microscopy measurements of the film thickness, is in the range $(2–10) \times 10^{-3}$ g/cm^3. Fast Fourier transforms of the foam high-resolution transmission electron microscopy (HRTEM, $\times 500\,000$) images revealed the existence of a structural period in the clusters with the space scales of $\approx 5.8 \pm 0.3$ Å.

In order to elucidate the electronic structure of the foam, optical absorption spectra, Raman spectra, and high-resolution electron energy loss spectra (EELS) were measured at room temperature, together with electrical resistivity in the temperature range from 80 K to 450 K. The optical absorption measurements provide an estimate of the optical band-gap, which is in the range from 0.5 to 0.7 eV, this being typical for sp^2-dominated *a*-C films [11]. However, the absorption measurements do not take into account the scattered portion of the incoming radiation which could be significant with this kind of structure, and the resulted optical band-gap of the foam could be in fact much higher.

The measured Raman spectra (632.8-nm excitation) are different to those obtained for laser-evaporated *a*-C films [5]. They show two separated broad peaks centred at (1341–1353) cm^{-1} (D-peak) and at (1569–1579) cm^{-1} (G-peak) which are attributed to graphitic sp^2 bonding (Fig. 3). In the same way as with the DLC films, the third peak with maximum at 1150–1160 cm^{-1}, related to the contribution of sp^3-bonded amorphous diamond [12–15], was required to fit the data. Nevertheless, the three peaks fitting never gave a satisfactory result, and a fourth peak at ≈ 1465 cm^{-1} was required, which could be identified with fullerenes in the carbon foam [16, 17].

Examples of the current–voltage (I–V) characteristics of the foam in the applied dc voltage range of ± 100 V at various

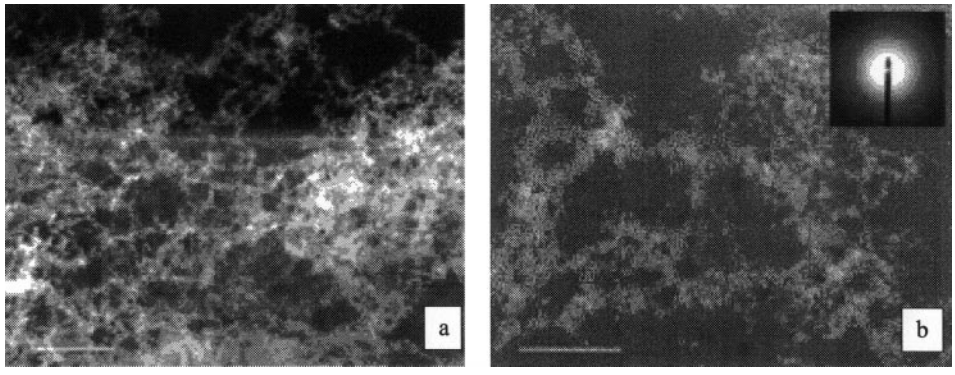

Fig. 2a,b. Scanning (**a**) and transmission (**b**) electron microscope images showing the free-standing carbon foam. The *bars* in the images are 1 μm (Fig. 2a) and 100 nm (Fig. 2b). The fractal structure is clearly seen in the high-resolution images of the foam, which consists of a network of interconnected carbon clusters of ≈ 6 nm in size. The transmission electron diffraction pattern in the Fig. 1b *inset* shows the very broad rings indicating the lack of a long-range 3D order in the foam

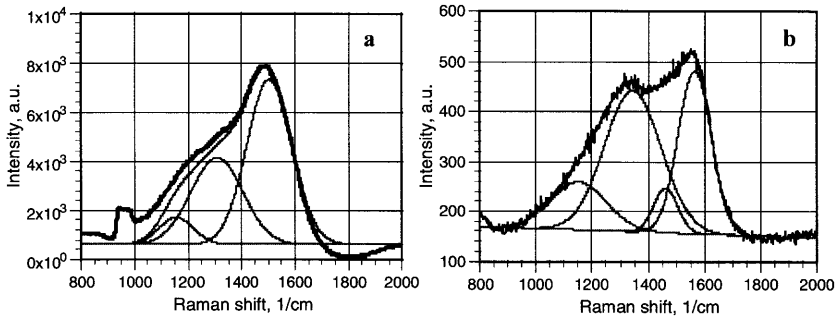

Fig. 3a,b. Raman spectra of amorphous carbon film (**a**) and carbon foam (**b**) in the 800–2000 cm^{-1} range, and the synthesised data resulting from contributing peak analysis

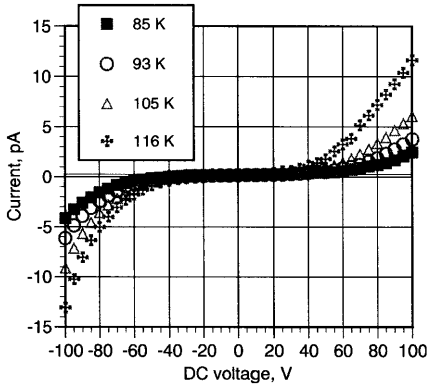

Fig. 4. Examples of nonlinear current–voltage (I–V) curves of the annealed carbon foam at various temperatures. The differential resistivity is about ten times higher in the low-voltage range within ±30 V than that at ±100 V

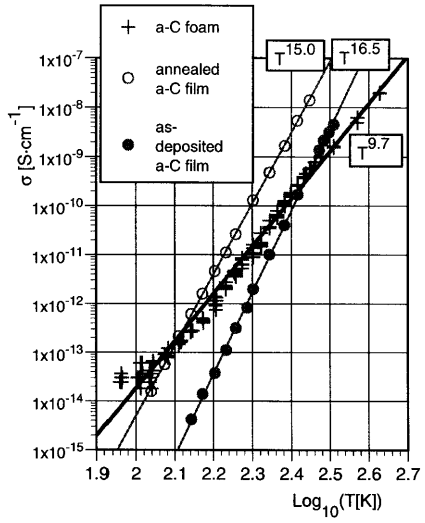

Fig. 5. Logarithmic temperature dependence of the dc conductivity of the carbon foam (*crosses*). For comparison, the dc conductivity for as-deposited (*closed circles*) and annealed (*open circles*) sputtered *a*-C films from [18] is shown. The T^n values for empirical description of the conductivity in the form are shown for each curve

temperatures from 85 K to 130 K are presented in Fig. 4. The I–V curves are symmetric with respect to voltage sign reversal. They are non-linear and demonstrate a voltage-dependent resistivity: the differential resistivity being approximately 10 times higher in the low-voltage region (within ±30 V) than in the high-voltage region (∼ ±100 V). The resistivity of the foam measured in the low-voltage region decreases with temperature from $\approx 10^{11}$ Ohm cm at 85 K to $\approx 10^{8}$ Ohm cm at room temperature (297 K) for the as-deposited foam, and from ≈ 14 Ohm cm at 85 K to $\approx 10^{9}$ Ohm cm at 297 K for the foam annealed at 450 K for 18 h. The temperature dependence of the dc conductivity on a double logarithmic scale is presented in Fig. 5. For comparison, results for an RF-sputtered *a*-C film [18] are shown on the same graph. Fitting the conductivity $\sigma(T)$ over a wide temperature range with a power law T^n gives $n = 9.5$–9.7 for the foam, compared to $n = 15$–17 for the RF-sputtered *a*-C films [18].

Summing up, the foam produced represents the new carbon structure which differs from the closest carbon relative—carbon aerogels [19] – by two orders of magnitude lower density and by eight orders of magnitude higher resistivity which is close to that of DLC dense films and diamond. In what follows we present the basic relationships, which govern the ablation process as well as considering the vapour state which is created within the evaporation chamber. From this we deduce the conditions for the carbon structure formation on the basis of the theoretical models and compare the predicted condition to those determined from the experiments. The ability to predict and control the carbon foam properties on the basis of the initial conditions created by laser ablation will allow us to discuss the possible formation mechanisms.

2 Theoretical background

The transition from the conventional low-repetition-rate laser ablation to the ultrafast regime involves an increase in the repetition rate and ideally a decrease in the pulse duration from the ns to ps or fs range. The latter change leads also to the change of the laser–target interaction mode and to the conditions for the optical breakdown of laser-produced vapours. Although the experiments reported here used ≈ 100-ns pulse duration in order to approach optimal evaporation conditions, there are clear advantages of using shorter pulses in particular to minimise contamination from particulates. In what follows we demonstrate how repetition rate and pulse duration affect the resulting laser plume parameters. First, we consider ionisation of the laser plume.

2.1 Ionisation state of the laser-ablated carbon vapours

Ionisation of the solid target and the dense laser-created vapour may occur by photoionisation, multiphoton ionisation, and by electron impact due to avalanche ionisation. As ionisation proceeds the vapour converts into a high-density plasma

whose properties can eventually dominate the physics of the laser–vapour interaction.

The number density of the electrons n_e created under the action of the laser electric field can be presented in general form [20, 21] as follows:

$$\frac{dn_e}{dt} = \frac{n_e(t)}{t_{ion}} + W_{mphi} - \left(\frac{dn_e}{dt}\right)_{loss} . \quad (1)$$

The first term represents ionisation by electron impact; the second relates to multiphoton ionisation; and the third describes the electron losses through diffusion, recombination, etc. Ionisation by electron impact is the most efficient process in a dense gas ($> 10^{18}\,cm^{-3}$) [21] and in dielectrics at laser intensities $\approx 10^9\,W/cm^2$ (wavelength of $\approx 1000\,nm$ [20]). This mechanism is also responsible for optical breakdown of the vapour and consequently for the vapour-to-plasma transition. Multiphoton ionisation dominates at high intensities and for short-wavelength lasers. It should be noted that multiphoton ionisation, as a threshold-free process, also creates the seed electrons for avalanche ionisation at low intensities. In what follows we neglect the losses and multiphoton process and estimate the contribution of avalanche ionisation to the plasma formation process at different intensities. In this case the number of electrons produced by the avalanche process during a laser pulse of duration, t_p, is as follows:

$$n_e = n_0 \exp\left(\frac{t_p}{t_{ion}}\right) . \quad (2)$$

Here t_{ion} is the time required for an electron to gain energy equal to the first ionisation potential J_1 [21]:

$$t_{ion} \approx J_1 \left(\frac{2\varepsilon_{osc}\omega^2\nu_{eff}}{\omega^2+\nu_{eff}^2}\right)^{-1} . \quad (3)$$

ε_{osc} is the energy of electron oscillations in the laser field with intensity I, frequency ω and wavelength λ; and ν_{eff} is the effective collision frequency of electrons. The oscillation energy of an electron in the laser radiation field E can be written:

$$\varepsilon_{osc}[eV] = \frac{e^2E^2}{4m\omega^2} = \frac{e^2}{4m\pi c^3} I\lambda^2 = 4.67\times10^{-14} I\left[\frac{W}{cm^2}\right]\lambda^2[\mu m] . \quad (4)$$

One can expect, in accordance with [22], that $\omega/\nu_{eff} \approx 1$. The condition for optical breakdown is taken conventionally to occur when the number density of electrons equals the critical density for the appropriate laser wavelength (the density whose electron plasma frequency equals that of the optical radiation). In the case considered it results in $n_e/n_0 \approx 10^{21}$. Combining (2), (3), and (4) and the above conditions one obtains the relationship between the laser pulse duration and intensity for breakdown in the following form for carbon vapour ($J_1 = 11.26\,eV$):

$$t_p[s] \times I\left[\frac{W}{cm^2}\right] \times \lambda^2[\mu m] = 6.6 . \quad (5)$$

One can see from (5) that for the wavelength of 1064 nm and $I = 10^9\,W/cm^2$ the transformation of carbon vapour to the plasma occurs after 5.8 ns. This estimate is in reasonable agreement with the experimental data on glass breakdown [20], with the measurements of the ionisation state in the experiments on carbon ablation by 120-ns laser pulse [3, 5], and with the previous studies [23, 24]. Therefore, for a 100-ns pulse at the intensity $10^9\,W/cm^2$, the laser radiation interacts with plasma most of the time over the pulse duration.

Comparison of the heat propagation depth $x_{heat} \approx (at)^{1/2}$ (a is the thermal diffusivity, $a = 4\times10^{-2}\,cm^2/s$ for graphite [4]) and the expansion length during the laser pulse, $x_{exp} \approx vt$, shows that in the case of a 100-ns pulse, the hydrodynamic flow from the target surface dominates the interaction, i.e. the expansion length exceeds any other length including heat conduction length $x_{exp} \gg x_{heat}$. In contrast, a 60-ps pulse interacts with a carbon target in a regime intermediate between the skin effect mode, which is characteristic for very short (< 1 ps) pulses [25], and the regime where the vapours are transparent [4, 26]. For longer pulses ($t_p > 100$ ps) one can neglect the time-dependent terms in the equation for the energy conservation. Hence, in the conditions of these experiments the familiar quasi-stationary description of the laser-created vapours is appropriate [27].

2.2 *The quasi-stationary model for expansion of the laser plume in the transition regime from a neutral vapour to plasma*

In what follows we estimate the laser plume parameters such as density, temperature, and evaporation rate, using the conventional quasi-stationary approximation. We assume that the evaporation of the target occurs in a thin layer near the vapour–solid interface where the laser radiation is absorbed. Therefore density, velocity, pressure, and temperature all change abruptly in an infinitesimally narrow zone near the solid–vapour interface. As a result, we are considering a situation well known in studies of laser–matter interactions when all material parameters at this interface are related to the absorbed laser intensity via conservation laws for mass, momentum, and energy.

Let us denote the initial target mass density ϱ_0; the pressure in the solid p_0; the vapour pressure p_1; vapour velocity v_1; vapour mass density ϱ_1; the specific energy of vapour ε_1; the velocity of vaporisation v_{evap}; and I_a is the absorbed laser intensity. The conservation laws on the solid–vapour boundary are then as follows:

$$\begin{aligned} -\varrho_0 v_{evap} &= \varrho_1(v_1 - v_{evap}) , \\ p_0 &= p_1 - \varrho_0 v_{evap} v_1 , \\ I_a &= -\varrho_0 v_{evap}\left(\varepsilon_1 + \frac{v_1^2}{2}\right) + p_1 v_1 . \end{aligned} \quad (6)$$

Usually, $v_1 \gg v_{evap}$ and it is assumed that the Jouget–Chapman condition at the jump is fulfilled. Let us treat the vapour as an ideal gas with the adiabatic exponent γ, and the sound velocity c_1. In what follows we take as usual $v_1 \approx c_1$. Thus, the equation of state for the vapour reads:

$$\begin{aligned} &\varepsilon_1 = \frac{1}{\gamma-1}\frac{p_1}{\varrho_1} + \Omega + \frac{\varepsilon_{ion}}{M} ; \\ &c_1^2 = \gamma\frac{p_1}{\varrho_1} = \gamma\frac{k_B T}{M} ; \\ &\varrho_1 = n_1 M ; \qquad \text{and} \qquad p_1 = n_1 k_B T . \end{aligned} \quad (7)$$

Here Ω[J/g] is the heat of vaporisation or binding energy per one atom; $\varepsilon_b = \Omega M$, where M is atomic weight in grams; and the ionisation losses per atom $\varepsilon_{ion} = \sum(\alpha_{ion})^i J_i$; here $(\alpha_{ion})^i$ is the ionisation rate and J_i is the i-th ionisation potential. Note, that the conservation of mass gives us an expression for the evaporation rate, R_{evap}. We can now present the set (6) in the following form:

$$\begin{aligned} -n_0 v_{evap} &\approx n_1 c_1 \equiv R_{evap} \\ p_0 &= (1+\gamma) n_1 k_B T \\ I_a &= n_1 c_1 \left\{ \frac{\gamma(1+\gamma)}{2(\gamma-1)} k_B T + \varepsilon_b + \varepsilon_{ion} \right\} , \end{aligned} \tag{8}$$

where $k_B T$ is the electron temperature. Making use of (7) one can express the evaporation rate through the absorbed intensity and surface temperature:

$$R_{evap} = n_1 c_1 = \frac{I_a}{\varepsilon_b + \varepsilon_{ion} + k_B T \frac{\gamma(1+\gamma)}{2(\gamma-1)}} . \tag{9}$$

One can see that two well-known limit cases immediately follow from the set (8). In the case of low intensities (low temperature, $\varepsilon_b \gg k_B T$) the characteristic density, n_1, can be expressed through an Arrenius-like formula [26–28]:

$$n_1 = \beta n_0 \left(\frac{c_0}{c_1} \right)^3 \exp\left\{ -\frac{\varepsilon_b}{k_B T} \right\} . \tag{10}$$

Hence, one arrives at the known laser–matter interaction regime where the vapours are transparent [4, 26]. The temperature dependence of the absorbed intensity can be calculated from the equation:

$$\frac{I_a}{I^*} = \left(\frac{\varepsilon_b}{k_B T} + \frac{\gamma(\gamma+1)}{2(\gamma-1)} \right) \exp\left\{ -\frac{\varepsilon_b}{k_B T} \right\} . \tag{11}$$

Here I^* is the characteristic intensity expressed through the target parameters alone:

$$I^* = \frac{\beta}{\gamma} \varrho_0 c_0^3 ; \tag{12}$$

$\beta \approx 10 - 30$ is a numerical constant, which should be determined from the relevant experiment [26].

In the limit of high laser intensities (8), (9), $k_B T \gg \{\varepsilon_b, \varepsilon_{ion,}\}$ and $n_1 = n_c$ (critical density for the given laser wavelength), one arrives at a high temperature laser plasma model [27–29].

The experiments on laser ablation for deposition of thin carbon films have shown [3, 5] that the laser-created plume is partly ionised. The UV spectra clearly demonstrated the presence of single and double ionised carbons but the ionisation rate was difficult to identify. The temperature measurements indicate that the vapour temperature lies in the range of $k_B T \approx 2$ eV, therefore suggesting the possibility of ionisation and, most probably, a low ionisation degree. Hence, one can assume that the interaction regime in high-repetition-rate laser ablation experiments is of a transitional nature between the regime where the vapours are transparent and the state of the pure laser–plasma interaction. One can see that in the regime of transparent vapours the characteristic vapour density grows with intensity. It, therefore, seems reasonable to suggest that in this transitional regime the vapour density near the target surface is close to the critical density, n_c. Thus, the energy conservation law in the form of (9) transforms to the following:

$$n_c c_1 = n_c \left(\frac{\gamma k_B T}{M} \right)^{1/2} = \frac{I_a}{\varepsilon_b + \varepsilon_{ion} + k_B T \frac{\gamma(\gamma+1)}{2(\gamma-1)}} . \tag{13}$$

Let us denote $\varepsilon_t = \varepsilon_b + \varepsilon_i$. Then the plasma temperature can be calculated ($\gamma = 5/3$ is the adiabatic constant) as the following:

$$x^{1/2} = \frac{\frac{I_a}{I^{**}}}{1 + \frac{10}{3} x} ; \qquad x = \frac{k_B T}{\varepsilon_t} . \tag{14}$$

Here I^{**} is a characteristic intensity for the transitional regime:

$$I^{**} = n_c \gamma^{1/2} \frac{\varepsilon_t^{3/2}}{M^{1/2}} . \tag{15}$$

Comparison of (12) and (15) for carbon ($M = 12$ a.m.u., $\varepsilon_b = 3.68$ eV, density $\varrho_0 = 2.25$ g/cm^3, $c_0 \approx 10^5$ cm/s; $\gamma = 5/3$) and $\lambda = 1.064\,\mu$m ($n_c = 1.16 \times 10^{21}$ cm^{-3}) gives $I^{**} = 4.8 \times 10^8$ W/cm^2, and $I^* = \beta \times 10^8$ W/cm^2. Note that for the case of full single ionisation the characteristic flux I^{**} increases by 8.26 times (for carbon).

Let us now compare the theoretical predictions for the parameters of the carbon plume with the experimental results. According to the measurements, the interaction of 1.064-μm, 10^9-W/cm^2, 120-ns 10-kHz laser with a graphite target results in a plume with an average temperature 1.5–6 eV and emitting lines characteristic of singly and doubly ionised carbon. Therefore the transitional model of (13)–(15) is applicable for the description of the plume properties. The calculations with $I^{**} = 4 \times 10^9$ W/cm^2 (assuming single ionisation) give $k_B T = 2$ eV, and for the case of low ionisation fraction ($I^{**} = 4.8 \times 10^8$ W/cm^2) one obtains $k_B T = 0.69$ eV. These temperatures are close to the maximum temperature during the single pulse. Therefore, according to the theory presented, the ionisation degree in the experimental conditions should be low.

For comparison, the estimates above suggest that in case of ultrafast evaporation with a 60-ps, 3×10^9 W/cm^2, 76-MHz laser, the plume should remain neutral [5]. Therefore, the most relevant theoretical model for the plume characterisation should be the model for transparent vapour of (11)–(12). In this case one obtains $k_B T = 1.84$ eV for the carbon vapours (which is T_{max}), or for the average temperature for 76 MHz repetition rate $\langle T \rangle = 0.135\, T_{max} = 0.248$ eV = 2880 K in a good fit to the measured 2500–3500 K temperature.

3 Deposition of carbon vapours at various ambient gas pressures

3.1 Conditions for carbon cluster formation in Ar

The formation of carbon cluster consists of several stages. The flow of atomic carbons is created by the laser ablation near the target surface but now the chamber is filled with an

inert ambient gas. As a result as the carbon plume expands, carbon atoms collide with the ambient gas atoms, diffuse through the gas, exchanging their energy, and finally cool down to the average carbon-gas temperature. Therefore, the number density and temperature of the carbon atoms (ions) change with the distance from the target, and therefore can be quite different in the regions near to the target compared to those at the substrate. Let us first describe the processes of collision and diffusion qualitatively.

3.1.1 Evaporation rate. As a first approximation, let us neglect the spatial and temporal distribution of carbon atoms in the chamber, taking the carbon atom number density averaged over the chamber volume at any moment of time. Then the carbon source can be presented as the following:

$$n\frac{\mathrm{d}n_{01}}{\mathrm{d}t} = \frac{R_{\mathrm{rep}}R_{\mathrm{evap}}S_{\mathrm{foc}}t_{\mathrm{p}}}{V_{\mathrm{chamber}}} \,. \tag{16}$$

For the experimental conditions with 10-kHz laser one obtains the number density rate of $\approx 10^{15}\,\mathrm{cm^{-3}s^{-1}}$.

3.1.2 Velocities of single carbon atoms and N-atomic clusters. The ablation of the carbon target produces carbon atoms with the average temperature of $\approx 2\,\mathrm{eV}$ ($v_{\mathrm{carbon}} = 3.1\times10^5\,\mathrm{cm/s}$). Initially, argon is at room temperature of 300 K ($v_{\mathrm{argon}} = 0.2\times10^5\,\mathrm{cm/s}$). Therefore, a single carbon atoms experiences velocity changes in the range $0.2\times10^5\,\mathrm{cm/s} < v_1 < 3.1\times10^5\,\mathrm{cm/s}$. If we assume as a threshold temperature for the beginning of a cluster formation 1200 K, then $v_{1200\mathrm{K}} = 0.64\times10^5\,\mathrm{cm/s}$. For a cluster comprising N carbons one may suggest $v_{\mathrm{cluster}} \approx v_1 N^{-1/2}$, assuming the equilibrium conditions.

3.1.3 Mean free path, collision time, and equilibration time. We assume a conventional geometric cross-section of $\sigma \approx 10^{-15}\,\mathrm{cm^2}$ for both C–Ar and C–C collisions. The number density of Ar in a chamber n_{Ar} was in the range from $3\times10^{16}\,\mathrm{cm^{-3}}$ (at 1 Torr) to $3\times10^{18}\,\mathrm{cm^{-3}}$ (at 100 Torr). This corresponds to the C–Ar, C–C collision length (or mean free path, $l \approx (n_{\mathrm{Ar}}\sigma)^{-1}$) from $3.3\times10^{-2}\,\mathrm{cm}$ to $3.3\times10^{-4}\,\mathrm{cm}$. The masses of colliding atoms are comparable; thus a carbon atom can lose a significant part of its energy even in a single collision. Hence, efficient energy equilibration occurs after only a few collisions: the carbon atoms cool and the argon atoms heat up. The typical collision time for a single carbon is $t_{\mathrm{coll}} \approx (n\sigma v)^{-1} = 3.3\times10^{-7}\,\mathrm{s}$ for 1 Torr, and $3.3\times10^{-9}\,\mathrm{s}$ for 100 Torr of argon. If we assume that complete equilibration needs up to ≈ 10 collisions, one can see that equilibration process takes from 10 to 100 ns.

For an N-atomic cluster the collisional geometric cross section increases as $R^2 \approx N^{2/3}$. Therefore, the mean free path decreases with a cluster size as $l_{\mathrm{cluster}} \approx N^{-2/3}$. Correspondingly, the collision time for N-atomic cluster scales up with N as $t_N \sim t_{\mathrm{coll}}N^{1/6}$. One can see that a single carbon experiences from 300 to 10^5 collisions during its diffusion path from the target to a substrate located at a distance $R_{\mathrm{t\text{–}s}} \approx 10\,\mathrm{cm}$.

3.1.4 Diffusion time. The main transport mechanism for a single carbon or cluster is the diffusion. The diffusion velocity and diffusion time to travel a distance L are:

$$D = \frac{lv}{3}\,; \qquad t_{\mathrm{diff}} = \frac{L^2_{\mathrm{diff}}}{D} = 3L^2 n\frac{\sigma}{v}\,. \tag{17}$$

Taking into account the previous equations one obtains the relationship between the diffusion time for a single carbon and for an N-atomic cluster:

$$t^{(N)}_{\mathrm{diff}} = N^{7/6}t^{(1)}_{\mathrm{diff}}\,. \tag{18}$$

The diffusion time for a single carbon ($v \approx 10^5\,\mathrm{cm/s}$) from target to substrate is: $t_{\mathrm{diff}} \approx 0.1\,\mathrm{s}$ at 1 Torr of Ar, and $t_{\mathrm{diff}} \approx 10\,\mathrm{s}$ for 100 Torr. If we assume that a 6-nm cluster, which consists of $\approx 4\times10^3$ carbon atoms is formed near the target, then the diffusion time in a 1-Torr argon gas from the target to substrate where the clusters were collected, must be in the order of $\approx 1.6\times10^3\,\mathrm{s}$.

3.1.5 Average temperature and density in the chamber. If we assume no consumption of evaporated carbons in the chamber, i.e. if the density and the temperature of single carbon atoms are lower than to form clusters, then both the partial density of carbon atoms and the average temperature for C–Ar mixture grow in time as follows:

$$\begin{aligned} n_1 &= \frac{\mathrm{d}n_{01}}{\mathrm{d}t}t\,, \\ T(t) &\approx \frac{T_{\mathrm{m}}\frac{\mathrm{d}n_{01}}{\mathrm{d}t}t + T_{\mathrm{Ar}}n_{\mathrm{Ar}}}{\frac{\mathrm{d}n_{01}}{\mathrm{d}t}t + n_{\mathrm{Ar}}}\,. \end{aligned} \tag{19}$$

This growth stops when the cluster formation process begins.

3.1.6 Characteristic time for N-atomic cluster formation. Let us consider the N-atomic cluster assembly in a C–Ar mixture under assumption that the main building process is dominated by single-atom attachment to a bigger cluster. The concentration of carbon atoms may be written as $n_1/(n_1+n_{\mathrm{Ar}})$. As it is shown below, the inequality holds at $n_1 \ll n_{\mathrm{Ar}}$ during the formation process. Hence, the atom concentration could be expressed as $\approx n_1/n_{\mathrm{Ar}}$. At the initial stage, far from the saturation, one can describe the cluster formation with the help of the following set of coupled chemical rate equations:

$$\frac{\mathrm{d}n_i}{\mathrm{d}t} = \frac{n_1^2}{n_1+n_{\mathrm{Ar}}}n_{i-1}\sigma_{i,i-1}v_{i,i-1} \qquad i = 2, 3....N\,. \tag{20}$$

Here n_1, n_i are the single-carbon number density and an i-atomic cluster density in $\mathrm{cm^{-3}}$; $\sigma_{i,i-1}$ is an attachment probability, and $v_{i,i-1}$ is the relative velocity. The set (20) can be solved by successive integration assuming that that the carbon-cluster attachment probability and relative velocity are he same for formation of large ($\mathrm{N} \gg 1$) clusters:

$$\langle\sigma_{i,i-1}\rangle \equiv \sigma\,; \qquad \langle v_{i,i-1}\rangle \equiv v\,. \tag{21}$$

The solution for (20) for the simplest case of the constant single carbon number density ($n_1 = \mathrm{constant}$) is:

$$n_N = \frac{n_1(\frac{t}{t_2})^{N-1}}{(N-1)!}\,; \qquad t_2 = \left(\frac{n_1^2}{n_{\mathrm{Ar}}}\sigma v\right)^{-1}\,; \tag{22}$$

then the time of formation one can express as follows:

$$t = \left(\frac{n_N}{n_1}\right)^{1/N-1} [(N-1)!]^{1/(N-1)}\, t_2 \,. \tag{23}$$

One shall note from (23) that for a large cluster ($N \approx 10^3 - -10^4$) this formation time is independent of the cluster number density due to the fact that $(n_N/n_1)^{1/(N-1)} \approx 1$. Making use of the Stirling formula for the factorial one can reduce (23) to the characteristic time of N-atomic cluster formation:

$$t_N \cong \frac{1}{e} N t_2 \,. \tag{24}$$

Here $e = 2.718$ is the base of the natural logarithm.

3.2 Carbon cluster formation process

3.2.1 Consumption rate. Let us now estimate the single atom consumption rate during the clusters formation process:

$$\left(\frac{\mathrm{d}n_i}{\mathrm{d}t}\right)_{\text{form}} = \sum_{i=2}^{N} \frac{\mathrm{d}n_i}{\mathrm{d}t} \,. \tag{25}$$

Taking for the cluster formation rate after (20) and (22) $\mathrm{d}n_i/\mathrm{d}t \approx e n_1/i t_2$, one obtains from (25):

$$\left(\frac{\mathrm{d}n_i}{\mathrm{d}t}\right)_{\text{form}} \approx \frac{n_1}{t_2} = \frac{n_1^3}{n_{\text{Ar}}} \sigma v \,. \tag{26}$$

One can easily see from (26) that for any reasonable laser ablation parameters the consumption rate of single carbon atoms far exceeds the ablation rate. Therefore, when the threshold temperature and density for the cluster formation is achieved the partial density of carbon atoms in a chamber begins to decrease until the consumption rate determined by (26) is balanced by the ablation rate from (16). This minimum carbon density can be obtained from the following equation:

$$\frac{\mathrm{d}n_{01}}{\mathrm{d}t} = \frac{n_1^3}{n_{\text{Ar}}} \sigma v \,; \qquad n_{1,\min} = \left(\frac{\frac{\mathrm{d}n_{01}}{\mathrm{d}t} n_{\text{Ar}}}{\sigma v}\right)^{1/3} \,. \tag{27}$$

For a 1-Torr Ar pressure in the chamber the minimum density equals to $6.69 \times 10^{13}\,\mathrm{cm}^{-3}$ whereas for a 100-Torr it constitutes $3.1 \times 10^{14}\,\mathrm{cm}^{-3}$, both values are significantly lower than the correspondent Ar density. The time-dependent carbon density in the chamber can be obtained by solving the following equation:

$$\frac{\mathrm{d}n_1}{\mathrm{d}t} = \frac{\mathrm{d}n_{01}}{\mathrm{d}t} - \frac{n_1^3}{n_{\text{Ar}}} \sigma v \,. \tag{28}$$

Most of the time the second term in (28) is much larger than the first one. An approximate solution of the truncated equation reads:

$$\tau_{\min} - \tau_{\text{thr}} = \frac{n_{\text{Ar}}}{2 n_{\text{thr}}^2} \left(\frac{n_{\text{thr}}^2}{n_{\min}^2} - 1\right) \,; \qquad \tau = \int_{t_{\text{thr}}}^{t} \sigma v \mathrm{d}t \,. \tag{29}$$

Equation (29) presents the time when the minimum density of carbons is achieved.

After some time the carbon density along with the reaction rate becomes low, and the cluster formation process terminates. At this moment the single carbons' number density starts to increase again due to evaporation, and the next cycle of cluster formation begins. We may somewhat arbitrarily suggest that the moment when the minimum density occurs coincides with the termination of cluster formation. In this scenario the cluster formation proceeds periodically, and the formation time equals to the period from the moment when the threshold achieved to the moment of the minimum density. Let us assume the threshold temperature to be $\approx 1200\,\mathrm{K}$. One can calculate from (17) that such a temperature is achieved $\approx 1\,\mathrm{s}$ after the beginning of the evaporation. At this moment the single carbon atom density equals $\approx 10^{15}\,\mathrm{cm}^{-3}$. The formation period can be readily estimated from (29) assuming σ and v are constant:

$$t_{\min} - t_{\text{thr}} = \frac{n_{\text{Ar}}}{2\sigma v n_{\text{thr}}^2} \left(\frac{n_{\text{thr}}^2}{n_{\min}^2} - 1\right) \,. \tag{30}$$

In view of $n_{\text{thr}} > n_{\min}$ for both Ar density limits one can present the cluster formation time in the following general form:

$$\Delta t_{\text{form}} \approx \frac{1}{2} \left(\frac{n_{\text{Ar}}}{\sigma v \left(\frac{\mathrm{d}n_{01}}{\mathrm{d}t}\right)_{01}^2}\right)^{1/3} \tag{31}$$

For $n_{\text{Ar}} = 3 \times 10^{16}\,\mathrm{cm}^{-3}$ and other parameters as above the estimate for the formation time is $\approx 3.3 \times 10^{-2}\,\mathrm{s}$. This time also determines the size of a cluster formed. Comparing (31) to (22), (24) one can calculate the maximum cluster size that may be formed during the formation time:

$$\Delta t_{\text{form}} \approx t_N \,; \qquad N \sim \frac{e}{2} n_1^2 \left(\frac{\sigma v}{n_{\text{a}} \frac{\mathrm{d}n_{01}}{\mathrm{d}t}}\right)^{2/3} \tag{32}$$

Taking $n_1 \approx 10^{15}\,\mathrm{cm}^{-3}$ we estimate the number of carbons in a maximum cluster being of several hundred which is in a qualitative agreement with the experimental observations (several thousands). We should stress that all the estimates have a qualitative character because we do not know the real attachment cross-sections, and hence we have used the geometric collisional cross-section value for the attachment cross-section.

3.2.2 Does the argon gas cool down during cluster formation? Let us estimate the cooling time for argon during the first period of formation process ($3.3 \times 10^{-2}\,\mathrm{s}$) with the use of conventional heat conduction equation. The thermal diffusion coefficient in accordance with the kinetic theory is of the same order of magnitude as the diffusion velocity of (17):

$$a = \frac{K}{C_{\text{p}} n_{\text{Ar}}} \approx \frac{lv}{3} \,.$$

Here κ is heat conduction coefficient in [J/(cm s K)], C_{p} is specific heat in [J/K], n_{a} is number density in cm^{-3}. Taking $v = 10^5\,\mathrm{cm/s}$, $\sigma \approx 10^{-15}\,\mathrm{cm}^2$, and $n_{\text{Ar}} = 3 \times 10^{16}\,\mathrm{cm}^{-3}$ (1 Torr of Ar) one obtains $a \approx 10^3\,\mathrm{cm}^2/\mathrm{s}$. The chamber walls

are at room temperature at the distance $L \approx 10$ cm from a substrate (assumed to be the formation region). Then the cooling time is as the following:

$$t_{\text{cool}} \approx \frac{L_{\text{diff}}^2}{a} ,$$

and $t_{\text{cool}} \approx 0.1$ s, i.e. the same order of magnitude as formation time (3.3×10^{-2} s). We may expect therefore that the argon temperature remains approximately at the formation temperature ($\approx 10^3$ K) at the end of the first formation period. It means that in the next period of heating the temperature of the mixture will be higher than in the first one hence allowing for the formation of sp^3-bonding along with the sp^2-bonding.

3.2.3 Suggested scenario of carbon cluster formation in a C−Ar *mixture created by a high-repetition-rate laser.* Laser ablation creates an almost continuous inflow of hot carbon atoms and ions with an average temperature of ≈ 2 eV into the experimental chamber. The shock wave generated by each pulse rapidly decelerates in the ambient gas atmosphere, and further propagation of hot carbons proceeds by diffusion. Initially the ambient gas is at room temperature. Hence, the continuous flow of carbon atoms heats the ambient gas and increases the partial density of carbons in the chamber. When the temperature and the carbon number density increase to the level when the carbon–carbon attachment probability becomes significant, the formation of carbonaceous clusters begins. The carbon consumption rate during this formation process significantly exceeds the evaporation rate by laser ablation. Therefore, the carbon number density rapidly decreases to the value when the formation process terminates. Continuing laser evaporation leads again to the increase of the carbon number density to the value sufficient to start the next cycle of cluster formation.

We suggest that the formation process comprises periodic heating and cluster formation stages with the time period dependent on the initial Ar density, the evaporation rate, and reaction rate which in turn is a function of the temperature and density of the atomic carbon. It is essential that during the short period of cluster formation (in comparison to the heating period) the argon gas does not cool down but maintains its temperature approximately equal to that required for cluster formation. Hence, starting from the second period the argon temperature along with the carbon temperature is higher than the temperature at the formation threshold, and this is believed to be sufficient for sp^2 bonding. Therefore, the higher temperature achieved during the following formation periods is sufficient for appearance of the sp^3 bonds along with the sp^2 bonding observed in the cluster-assembled carbon foam.

The maximum number of atoms N in a cluster relates, from the kinetic viewpoint, to the diffusion time of the already formed cluster with m atoms. The diffusion time required for m-cluster to travel the distance l to the point of N-cluster formation defined from (18) can not exceed the N-cluster formation time defined from (24). Taking 3.3×10^{-2} s from the (22) and (24) and making use of (3) for $n_{\text{Ar}} = 3 \times 10^{16}\,\text{cm}^{-3}$ one obtains: $m^{7/6} l^2[\text{cm}] \approx 33$. Therefore, at 1 Torr of Ar the very big clusters of tens of carbons can arrive at the N-cluster formation point from the distances up to $l \approx 1$ cm.

4 Conclusions

Ultrafast laser ablation with high-repetition-rate ps lasers leads to a number of new opportunities for the thin film formation and for the creation of nanostructured materials. First, due to a low number of atoms evaporated per single laser pulse the problem of particulate formation in the laser plume could be completely resolved. This removes the main disadvantage of laser ablation with conventional low-repetition-rate powerful lasers. Second, the transition from a ns pulse range to the ps region leads to a significant increase of evaporation rate and consequently, an increase in deposition rate, providing the laser intensity is optimal for the particular target material. Third, the high repetition rate leads to an increase of the average surface temperature and pressure at the substrate during the interaction time. Both parameters depend on the laser intensity during the single pulse and the pulse repetition rate. Therefore, an increase of intensity allows the optimum conditions for graphite–diamond phase transition to be approached.

Carbon-carbon interaction in the Ar ambient (or, any non-reactive gas) leads to the formation of a new carbonaceous material – a diamond-like low-density carbon foam. This foam has typical semiconductor properties: the band gap is 0.1–0.5 eV, the resistivity is 10^9–10^{12} Ohm cm depending on the Ar gas density, and the semiconductor-like dependence of the resistivity on temperature. The bond structure of this material is also unusual: it has from 15% to 45% of sp^3 bonds, which allows us to call it the "diamond-like carbon foam" by analogy with the DLC films. By analogy with the amorphous carbon and silicon, one can suggest that sp^2 (graphite-like) structures can be mainly attributed to the cluster sites, whereas the sp^3 bonds are located in the connections between the clusters.

Theoretical predictions of the parameters of the carbon vapour in the laser-ablated plume and the process of carbon vapour diffusion through the ambient gas, allow us to propose a self-consistent periodic model leading to the formation of the carbon clusters in the experimental chamber. The periodicity of the formation process is due to the balance between the density and temperature of the arriving atoms from the target on the one hand and the consumption of the carbon atoms due to the process of cluster formation on the other hand. The presented kinetic analysis of the carbon vapour in the Ar ambient demonstrates qualitative agreement between the predicted laser plume parameters and those measured in the experiments. This analysis could be applied to a variety of nano-sized cluster formation processes based on the laser ablation, such as production of carbon nanotubes and other nanostructured materials.

It was demonstrated that the high-repetition-rate laser ablation is a new flexible and controllable tool producing the continuous flow of atomic or ionised vapours with the well-characterised density and temperature for formation of thin films and new nanostructures.

Acknowledgements. We are very thankful to S.T. Hyde and D.R. McKenzie for valuable and stimulating discussions. We gratefully acknowledge our colleagues who helped us to perform a number of the DLC foam measurements: R.G. Elliman (resistivity and density measurements), S. Bulcock (EELS sp^3/sp^2 ratio), J. Fitz Gerald (transmission electron microscopy), N.J. Welham (surface area measurements), and T.J. Senden (mass spectrometry). A.V.R. acknowledges support from the Australian Research Council

through a Queen Elizabeth II Fellowship, and E.G.G. acknowledges support from CONACYT of Mexico.

References

1. H.W. Kroto, J.R. Heath, S.C. O'Brien, R.F. Curl, R.E. Smalley: Nature **318**, 162 (1985)
2. A. Tess, R.S. Lee, P. Nikolaev, H. Dai, P. Petit, J. Robert, C. Xu, Y.H. Lee, S.G. Kim, A.G. Rinzler, D.T. Colbert, G.E. Scuseria, D. Tomanek, J.E. Fisher, R.E. Smalley: Science **273**, 483 (1996)
3. A.V. Rode, E.G. Gamaly, B. Luther-Davies: In XX International Quantum Electronics Conference, Sydney, Australia, 14–19 July 1996, OSA Technical Digest Series (Optical Society of America, Washington D.C. 1996) p. 137; A.V. Rode, E.G. Gamaly, B. Luther-Davies: In XI Australian Optical Society Conference Book of Abstracts, Adelaide, Australia, 10–12 December 1997(unpublished), p. W4; E.G. Gamaly, A.V. Rode: In *High-Power Laser Ablation*, ed. by C.R. Phipps, Proc. SPIE **3343**, 847 (1998); A.V. Rode, Luther-Davies, E.G. Gamaly: In *High-Power Laser Ablation*, ed. by C.R. Phipps, Proc. SPIE **3343**, 903 (1998)
4. E.G. Gamaly, A.V. Rode, B. Luther-Davies: J. Appl. Phys. **85**(8), 4213 (1999)
5. A.V. Rode, E.G. Gamaly, B. Luther-Davies: J. Appl. Phys. **85**(8), 4222 (1999)
6. O. Pierson: *Handbook of Carbon, Graphite, Diamond and Fullerenes* (Noyes Park Ridge 1993)
7. S. Acquaviva, A.P. Caricato, M.L. de Giorgi, A. Luches, A. Perrone: Appl. Surf. Sci. **109/110**, 408 (1997)
8. C. Vivien, J. Hermann, A. Perrone, C. Boulmer-Leborgne, A. Luches: J. Phys. D: Appl. Phys. **31**, 1263 (1998)
9. X. Chen, J. Mazumder, A. Purohit: Appl. Phys. A **52**, 328 (1991)
10. R.W.B. Pearse, A.G. Gaydon: *The Identification of Molecular Spectra* 4th edn.(Chapman and Hall, London; Wiley, New York 1976)
11. N. Savvides: J. Appl. Phys. **59**, 4133 (1986)
12. P.R. Chalker: In *Diamond and Diamond-Like Films and Coatings*, ed. by R.E. Clausing, L.L. Horton, J.C. Angus, P. Koidl (Plenum Press, New York 1991) p. 127; P.K. Bachmann, D.U. Wiechert: ibid. p. 677
13. J. Schwan, S. Ulrich, H. Roth, H. Ehrhardt, S.R.P. Silva, J. Robertson, R. Samlenski, R. Brenn: J. Appl. Phys. **79**, 1416 (1996)
14. V.I. Merculov, J.S. Lannin, C.H. Munro, S.A. Asher, V.S. Veerasamy, W.I. Milne: Phys. Rev. Lett. **78**, 4869 (1997)
15. C.Z. Wang, K.M. Ho: Phys. Rev. Lett. **71**, 1184 (1993)
16. P.C. Eklund, J.M. Holden, R.A. Jishi: Carbon **33**, 959 (1995)
17. B. Pietzak, J. Erxmeyer, T.A. Murphy, D. Nagengast, B. Mertesacker, A. Weidinger, K.W. Brzezinska: In *Physicsand Chemistry of Fullerenes and Derivatives*, ed. by H. Kuzmany, J. Fink, M. Mehring, S. Roth (World Scientific, Singapore 1995) p. 467
18. K. Shimakawa, K. Miyake: Phys. Rev. B **39**, 7578 (1989)
19. A.W.P. Fung, Z. Wang, K. Lu, M.S. Dresselhaus, R.W. Pekala: J. Mater. Res. **8**, 1875 (1993)
20. D. Du, X. Liu, G. Korn, J. Squier, G. Mourou: Appl. Phys. Lett. **64**, 3071 (1994)
21. Y.P. Raizer: *Gas Discharge Physics* (Springer, Berlin, Heidelberg 1991)
22. E. Yablonovitch, N. Blombergen: Phys. Rev. Lett. **29**, 907 (1972)
23. A.A. Puretzky, D.B. Geohegan, G.E. Jelison Jr., M.M. McGibbon: Appl. Surf. Sci. **96-98**, 859 (1996)
24. P.P. Pronko, P.A. Van Rompay, R.K. Singh, F. Qian, D. Du, X. Liu: Mat. Res. Soc. Symp. Proc. **397**, 45 (1998)
25. B. Luther-Davies, E.G. Gamaly, Y. Wang, A. Rode, V.T. Tikhonchuk: Sov. J. Quantum Electron. **22**, 289 (1991)
26. Y.V. Afanasiev, V.A. Isakov, I.N. Zavestovskaya, B.N. Chichkov, F. von Alvensleben, H. Welling: Appl. Phys. A **64**, 561 (1997)
27. Y.V. Afanasiev, O.N. Krokhin: *Gasdynamic Theory of Laser–Solid Interaction*, in P.N. Lebedev Institute Proceedings, v. 52, Nauka, Moscow, 1970; Y.V. Afanasiev, E.G. Gamaly, O.N. Krokhin, V.B. Rozanov: Sov. Phys. JETP **44**, 311 (1976)
28. Y.V. Afanasiev, O.N. Krokhin: High temperature plasma phenomena during the powerful laser-matter interaction, in *Physics of High Energy Density* (Proceedings of the International School of Physics "Enrico Fermi") Course XLVIII, ed. by P. Calderola, H. Knoepfel (Academic Press, New York, London 1971)
29. W.L. Kruer: *The Physics of Laser Plasma Interaction* (Addison Wesley, New York 1987)